crystals

MDPI

Communication

# Generalized Methodology for Inserting Metal Heteroatoms into the Layered Zeolite Precursor RUB-36 by Interlayer Expansion

**Chaoqun Bian [1], Xiao Wang [2], Lan Yu [1], Fen Zhang [3], Jie Zhang [1], Zhengxin Fei [1,*], Jianping Qiu [1,*] and Longfeng Zhu [2,*]**

1 Pharmaceutical and Material Engineering School, Jinhua Polytechnic, Jinhua 321000, China; bian00@zju.edu.cn (C.B.); 20101053@jhc.edu.cn (L.Y.); 20050635@jhc.edu.cn (J.Z.)
2 College of Biological, Chemical Sciences and Engineering, Jiaxing University, Jiaxing 314001, China; wxxx0225@zjxu.edu.cn
3 Institute of Applied Chemistry, Jiangxi Academy of Sciences, Nanchang 330096, China; 11437052@zju.edu.cn
* Correspondence: feizhengxin@jhc.edu.cn (Z.F.); jianpingqiu@jhc.edu.cn (J.Q.); zhulf1988@mail.zjxu.edu.cn (L.Z); Tel.: +86-579-8226-4066 (Z.F. & J.Q.); +86-573-8364-0131(L.Z.)

Received: 27 May 2020; Accepted: 18 June 2020; Published: 21 June 2020

**Abstract:** The incorporation of metal heteroatoms into zeolites is an effective modification strategy for enhancing their catalytic performance. Herein, for the first time we report a generalized methodology for inserting metal heteroatoms (such as Sn, Fe, Zn, and Co) into the layered zeolite precursor RUB-36 via interlayer expansion by using the corresponding metal acetylacetate salt. Through this generalized methodology, Sn-JHP-1, Fe-JHP-1, Zn-JHP-1 and Co-JHP-1 zeolites could be successfully prepared by the reaction of RUB-36 and corresponding metal acetylacetate salt at 180 °C for 24 h in the presence of HCl solution. As a typical example, Sn-JHP-1 and calcined Sn-JHP-1 (Sn-JHP-2) zeolite is well characterized by the X-ray diffraction (XRD), diffuse reflectance ultraviolet-visible (UV-Vis), inductively coupled plasma (ICP), $N_2$ sorption, temperature-programmed-desorption of ammonia ($NH_3$-TPD) and X-ray photoelectron spectroscopy (XPS) techniques, which confirm the expansion of adjacent interlayers and thus the incorporation of isolated Sn sites within the zeolite structure. Notably, the obtained Sn-JHP-2 zeolite sample shows enhanced catalytic performance in the conversion of glucose to levulinic acid (LA) reaction.

**Keywords:** RUB-36 zeolite precursor; interlayer expansion; metal heteroatoms; isolated metal species

## 1. Introduction

Zeolites are considered as one of the most important porous catalysts in the process of industrial production due to their crystalline structures, large surface area, excellent stability and uniform pore channels [1–3]. Generally, the introduction of metal heteroatoms into zeolites is an effective modification approach for tuning their functionality [4–6]. Therefore, zeolites with metal heteroatoms are capable of fulfilling the practical requirements of catalytic application, and thus have attracted increasing attention in the past years [7–9]. For example, Hong et al., obtained Fe-UZM-35 zeolite catalyst by ion-exchange methodology, and this zeolite catalyst exhibited excellent low-temperature selective catalytic reduction (SCR) activity [10]; Wu et al., synthesized Sn-Beta by interzeolite conversion from Sn-ITQ-1, which demonstrated remarkable potential in various biomass conversion reactions [11]; Wang et al., reported the RhMn@S-1 catalysts that exhibit high efficacy for the $C_2$-oxygenates production from syngas [12].

Layered zeolites precursor, such as MWW, PREFER and RUB-39, would be a typical class of microporous zeolites after high-temperature calcination, which also plays a critical role in the industrial

applications [13–15]. Recently, the interlayer expansion reaction has been reported as a new and efficient methodology for synthesis of novel zeolites by the treatment of the above zeolites precursor [16–18]. Dichlorodimethylsilane (DCDMS) or diethoxydimethysilane [$Me_2Si(OEt)_2$], as interlayer expansion agents, provide an Si source for the interlayer space with the replacement of the organic structure directing agent (OSDA). Notably, the insertion of Si atoms increases the pore size of the original samples. For examples, Gies et al., obtained a new microporous structure named as COE-2 through the interlayer expansion of layered zeolite precursor RUB-39 [19]; Tatsumi et al., prepared a novel titanosilicate catalyst, which exhibited extraordinary catalytic ability, from a Ti-MWW precursor via the interlayer expansion method [20].

RUB-36, discovered by Gies et al., is a layered silicate zeolite precursor [21]. After the calcination of RUB-36 zeolite precursor at high temperature, RUB-37 zeolite with the CDO-type structure could be successfully obtained [22]. Notably, the substitution of Al and Ti for Si in the zeolite structure has been reported, and thus gives an active microporous catalyst [22,23]. For example, Yilmaz et al., reported a new aluminosilicate via the interlayer expansion reaction using Al-RUB-36, which exhibited excellent catalytic activity. Recently, Dirk E. De Vos et al., found a new interlayer expansion agent, Fe chloride, as a replacement of DCDMS, to fill the linking sites between the layers [24,25]. As a result, the insertion of Fe in the zeolite structure was successful via the interlayer expansion reaction for the first time. However, the insertion of other metal heteroatoms, such as Sn and Co, in the zeolite framework by this method is still unclear.

More recently, we have reported the interlayer expansion of the COK-5 zeolite by using an Sn salt, bis(2,4-pentanedionate)-dichlorotin [$Sn(acac)_2Cl_2$] [26]. Very interestingly, the obtained sample, containing tin species, was catalytically active. The successful synthesis of Sn-containing zeolites by the interlayer expansion reaction is potentially significant for catalytic applications.

Herein, we report a generalized methodology for the insertion of heteroatoms (such as Sn, Fe, Zn, and Co) into a layered zeolite precursor RUB-36 by interlayer expansion. RUB-36 zeolite precursor, as a 2D lamellar precursor, is treated individually with $Sn(acac)_2Cl_2$, iron acetylacetonate [$Fe(acac)_3$], bis(2,4-pentanedionato)zinc [$Zn(acac)_2$], and cobalt acetylacetonate [$Co(acac)_2$] at 180 °C for 24 h, and thus forms the products of Sn-JHP-1, Fe-JHP-1, Zn-JHP-1, and Co-JHP-1 respectively. As a typical example, the obtained Sn-JHP-1 zeolite and calcined Sn-JHP-1 (Sn-JHP-2) are investigated in detail.

Various characterizations, including X-ray diffraction (XRD), inductively coupled plasma (ICP), diffuse reflectance ultraviolet-visible (UV-Vis) spectroscopy, X-ray photoelectron spectroscopy (XPS) and temperature-programmed-desorption of ammonia ($NH_3$-TPD) techniques, confirm the incorporation of isolated Sn sites in the zeolite structure. Very importantly, the obtained Sn-JHP-2 zeolite after the high temperature calcination displays excellent catalytic performance in the conversion of glucose to levulinic acid (LA) reaction.

## 2. Results and Discussion

Figure 1 shows the schematic diagram of the topological conversion of layered RUB-36 to RUB-37 zeolite, layered Sn-JHP-1 and Sn-JHP-2 zeolite. After calcination of the OSDA (dimethyldiethyl ammonium cation) and thus the condensation of silanol between the neighboring layers, the CDO type zeolite (RUB-37) can be obtained. In addition, layered Sn-JHP-1 is synthesized by insertion of Sn species through interlayer expansion reaction, which creates a novel material with catalytically active sites linking the layers. Moreover, the condensation product is denoted as Sn-JHP-2 zeolite.

Figure 2 shows the XRD patterns of RUB-36, RUB-37, Sn-JHP-1, and Sn-JHP-2 samples. The first peak in the XRD pattern of RUB-36 (Figure 2a) is at about 8.14°, whereas the following treatment with $Sn(acac)_2Cl_2$ gives Sn-JHP-1 (Figure 2c) with the first peak at about 7.56°, indicating the increase in the interlayer distance, which is attributed to the insertion of Sn sites between the neighboring layers. In contrast, the first peak of RUB-37 shifts to 9.76° (Figure 2b), indicating the condensation of silica species between the layers due to the removal of the OSDA. This phenomenon was similarly observed for Sn-JHP-1 (7.56°, Figure 2c) and Sn-JHP-2 (7.90°, Figure 2d). Moreover, the first peak of Sn-JHP-2

zeolite exhibits a smaller shift than that of the RUB-37 zeolite, confirming the connectivity between the Sn and the zeolite framework. From the ICP data, the Si/Sn ratio was determined to be 160, as shown in Table 1.

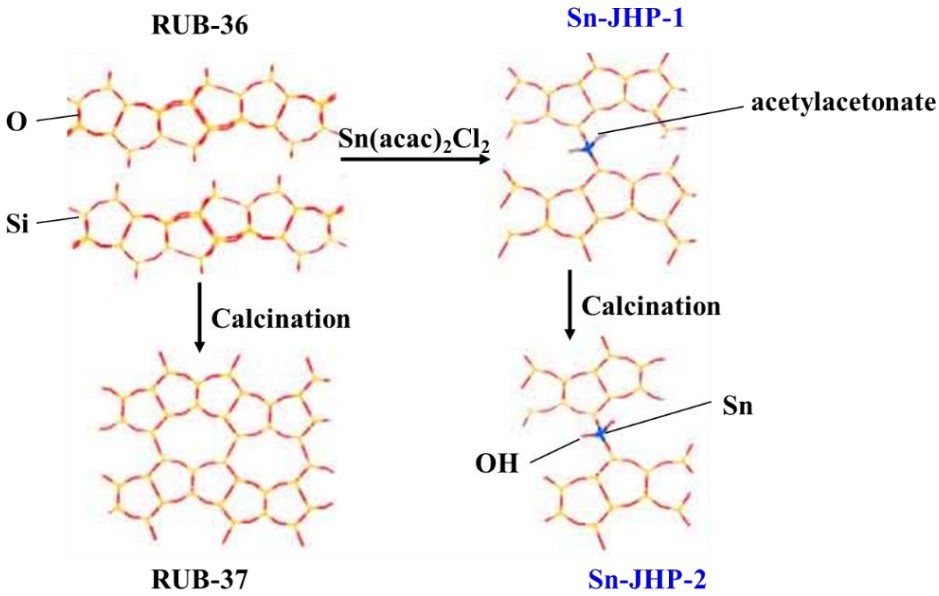


**Figure 1.** Schematic diagram of topological conversion of layered RUB-36 to RUB-37, Sn-JHP-1 and Sn-JHP-2.

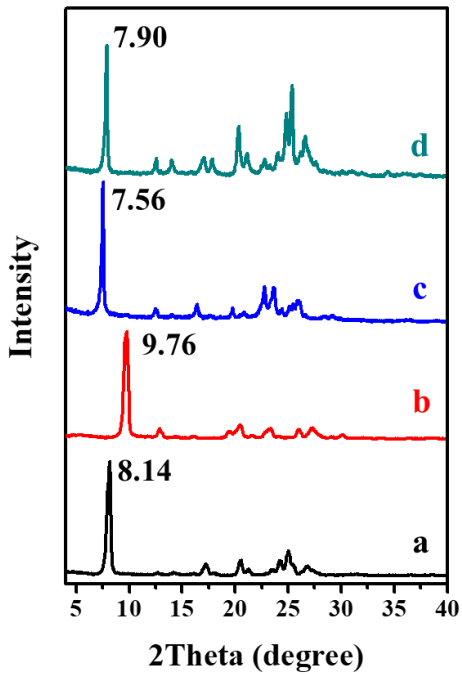


**Figure 2.** XRD patterns of (**a**) RUB-36, (**b**) RUB-37, (**c**) Sn-JHP-1 and (**d**) Sn-JHP-2.

**Table 1.** Parameters of the samples.

| Sample | BET Surface Area ($m^2g^{-1}$) | Micropore Volume ($cm^3g^{-1}$) | Si/Sn |
|---|---|---|---|
| RUB-37 | 288 | 0.12 | ∞ |
| Sn-JHP-2 | 362 | 0.17 | 160 |

Figure 3 gives the SEM images of RUB-36, RUB-37, Sn-JHP-1, and Sn-JHP-2 samples. All of the samples present similar morphology. Therefore, it could be concluded that the treatment does not affect the morphology of the sample.

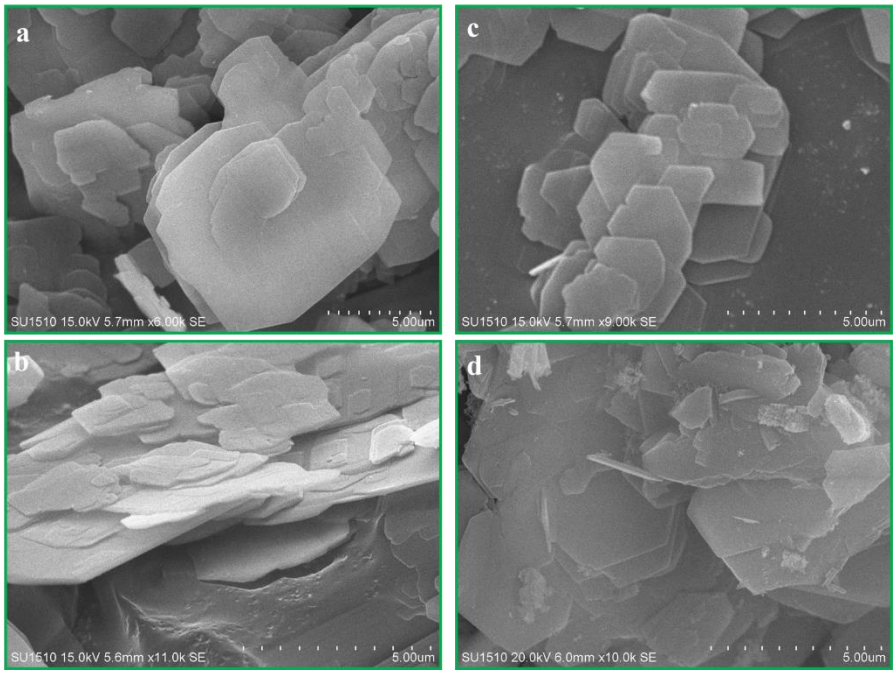


**Figure 3.** SEM images of (**a**) RUB-36, (**b**) RUB-37, (**c**) Sn-JHP-1 and (**d**) Sn-JHP-2.

Figure 4 displays the $N_2$ sorption isotherms of (a) RUB-37 and (b) Sn-JHP-2, which gives the related parameters, as shown in Table 1. Very interestingly, Sn-JHP-2 exhibits larger BET surface area (362 $m^2g^{-1}$) and micropore volume (0.17 $cm^3g^{-1}$) than that of RUB-37 (288 $m^2g^{-1}$, 0.12 $cm^3g^{-1}$), validating the interlayer expansion successfully.

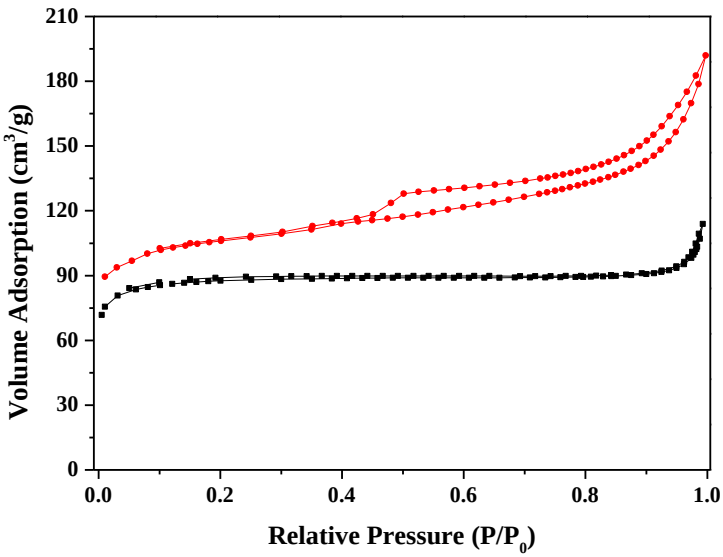


**Figure 4.** $N_2$ sorption isotherms of (**a**) RUB-37 and (**b**) Sn-JHP-2.

Figure 5 shows the UV-Vis spectra of (a) RUB-37, (b) Sn-JHP-1 and (c) Sn-JHP-2. From Figure 5, the obvious peaks in the RUB-37 sample are not observed due to the fact that no Sn is present. On the contrary, both Sn-JHP-1 and Sn-JHP-2 samples contain one major peak at approximately 240 nm.

This phenomenon is reasonably assigned to isolated tin species in the samples, in good agreement with the reported literatures [26,27].

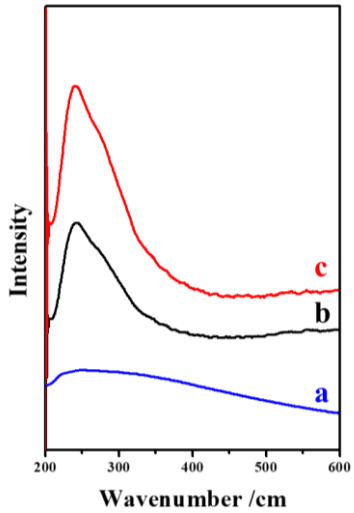


**Figure 5.** UV-Vis spectra of (**a**) RUB-37, (**b**) Sn-JHP-1 and (**c**) Sn-JHP-2.

Figure 6 shows the Sn $3d_{5/2}$ and $3d_{3/2}$ spectrum of the Sn-JHP-2, giving the binding energies of 486.9 eV and 495.7 eV respectively, which are clearly higher than the binding energies of the $SnO_2$ crystals (485.8 eV and 494.4 eV) [28,29]. This result confirms the insertion of isolated Sn sites between adjacent interlayers.

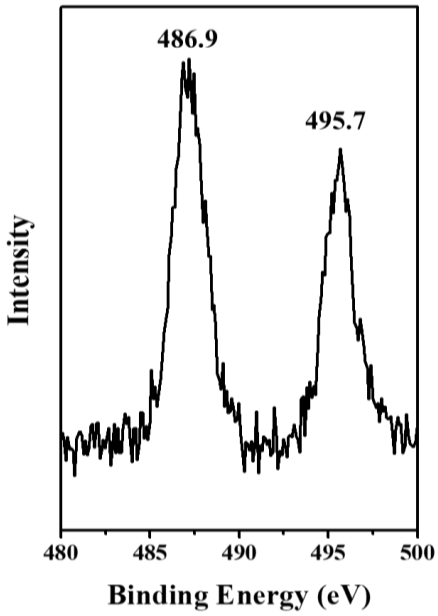


**Figure 6.** Sn $3d_{5/2}$ and $3d_{3/2}$ spectrum of the Sn-JHP-2.

Figure 7 shows the temperature-programmed-desorption of ammonia ($NH_3$-TPD) curves of (a) RUB-37 and (b) Sn-JHP-2. Obviously, Sn-JHP-2 has higher acid content than that of RUB-37 owing to the contribution of Sn species in the zeolite (Si/Sn = 160). Thus, the Sn-JHP-2 with more acidic sites would be helpful for the catalytic performance.

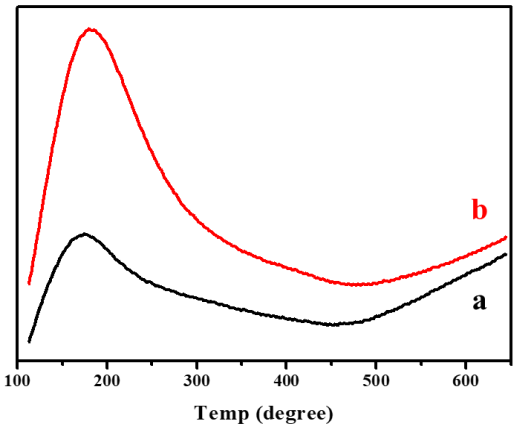


**Figure 7.** $NH_3$-TPD curves of (**a**) RUB-37 and (**b**) Sn-JHP-2.

Furthermore, the catalytic performance of RUB-37 and Sn-JHP-2 are tested by the conversion of glucose to levulinic acid (LA) reaction [30,31]. Generally, the transformation of glucose to LA is catalyzed by Bronsted- and Lewis-acid sites of the materials, and the ionic liquid media could retain the stability of acidic sites of the materials in the process of reaction, which has been widely reported in the literature [32,33]. In the process of reaction, the RUB-37 gives very low LA yields (1.3%) due to the absence of acidic sites. In contrast, the LA yields increase to 61.3% when Sn-JHP-2 is employed. The isolated Sn sites connected with the zeolite framework are hence considered to be catalytically active sites, giving the excellent catalytic performance. This performance is also remarkable compared with that of other catalysts such as boric acid (42%) [34], $Al_2O_3$ (49.7%) [35] and tin phosphate (58.3%) [36]. The above catalyst is also analyzed after reaction, which is named as Sn-JHP-2-r. The XRD pattern of Sn-JHP-2-r (Figure S1) shows that the sample still exists as a perfect zeolite structure. ICP analysis displays that the Si/Sn ratio of Sn-JHP-2-r is at about 167, suggesting no Sn species loss in the catalyst after reaction.

Similarly, Zn-JHP-1, Fe-JHP-1, and Co-JHP-1 samples are also successfully synthesized via the same method, confirming its universality of insertion metal heteroatoms into the layered zeolite precursor RUB-36 by interlayer expansion. Figure 8 shows the XRD patterns and UV-Vis spectra of (a) Zn-JHP-1, (b) Fe-JHP-1 and (c) Co-JHP-1. All of the as-synthesized samples exhibit peaks with lower angles (approximately 7.6°) in their XRD patterns than that of the RUB-36 sample, which are also caused by the insertion of the metal species between the neighboring layers. Correspondingly, the UV-Vis spectra of all of the samples further confirm the insertion of heteroatoms (Zn, Fe, and Co) in the zeolite framework, in good agreement with the results reported in the recent literature [24,36–40].

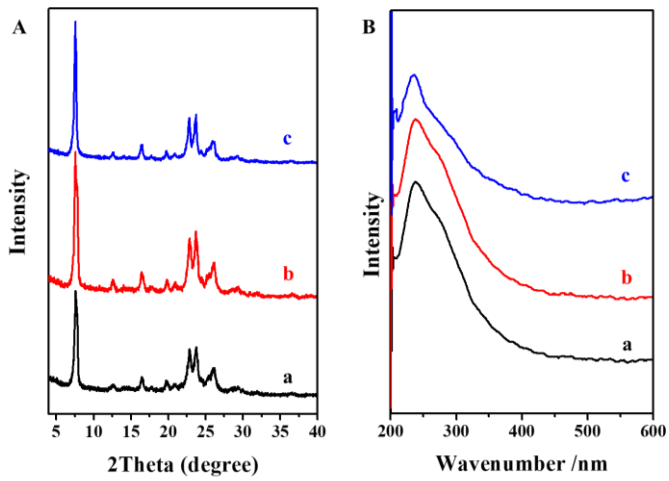


**Figure 8.** (**A**) XRD patterns and (**B**) UV-Vis spectra of (**a**) Zn-JHP-1, (**b**) Fe-JHP-1 and (**c**) Co-JHP-1.

## 3. Materials and Methods

### *3.1. Materials*

The following chemicals were utilized: iron acetylacetonate (AR, Aladdin Chemistry Co., Ltd. Shanghai, China), bis(2,4-pentanedionato)zinc (AR, Aladdin Chemistry Co., Ltd. Shanghai, China), cobalt acetylacetonate (AR, Aladdin Chemistry Co., Ltd. Shanghai, China), bis(2,4-pentanedionate)-dichlorotin (AR, Aladdin Chemistry Co., Ltd. Shanghai, China), and hydrochloric acid (AR, Sinopharm Chemical Reagent Co., Ltd. Shanghai, China). RUB-36 zeolites were supplied by BASF SE. All the chemicals were used directly without further purification.

### *3.2. Synthesis*

In a typical example for synthesis of Sn-JHP-1 and Sn-JHP-2, 0.2 g RUB-36 zeolite, 10 mL HCl (0.7 M) and 0.026 g $Sn(acac)_2Cl_2$ were stirred for 4 h at room temperature. The mixture was then transferred into a stainless steel reaction vessel, sealed and heated at 180 °C for 24 h. After filtration and drying, the white power could be obtained, which was named as Sn-JHP-1. After the calcination at 550 °C for 5 h, the final product could be obtained, which was named as Sn-JHP-2.

The typical examples for synthesis of Zn-JHP-1, calcined Zn-JHP-1 (Zn-JHP-2), Fe-JHP-1, calcined Fe-JHP-1 (Fe-JHP-2), Co-JHP-1 and calcined Co-JHP-1 (Co-JHP-2) are shown in the supporting information.

### *3.3. Methods*

XRD data were measured at room temperature with a Rigaku Ultimate VI X-ray diffractometer (40 kV, 40 mA) using CuKα (λ = 1.5406 Å) radiation. SEM experiments were carried out on Hitachi SU-8010 electron microscopes. The sample composition was determined by ICP with a Perkin-Elmer 3300DV emission spectrometer. UV-Vis analysis, using $BaSO_4$ as the internal standard sample, was performed on a Perkin-Elmer Lambda 20 spectrometer. XPS data were measured using a Thermo ESCALAB 250 with Al K irradiation at θ = 90° for the X-ray source, and the binding energies were measured by using the C 1s peak at 284.9 eV. $N_2$ sorption experiments were performed on a Micromeritics TriStar II at −196 °C.

### *3.4. Catalytic Test*

As a typical run for an $NH_3$-TPD test, the catalyst (0.1 g, 40–60 mesh) was treated at 400 °C in a He flow for 60 min, followed by the adsorption of $NH_3$ at 100 °C for 60 min. After saturation, the catalyst was purged by He flow for 30 min. Then, desorption of $NH_3$ was carried out from 100 to 700 °C with a heating rate of 10 °C/min.

As a typical run for a catalytic test, 1 mmol of glucose, 1.5 g of 1-ethyl-3-methylimidazolium chlorine ($EMIM^+Cl^-$) and 30 mg of Sn-JHP-2 samples were added, and mixed and stirred together at 110 °C for 2 h. Following extraction, the product was identified according to the known standards and analyzed by gas chromatography.

## 4. Conclusions

In summary, we have demonstrated a generalized methodology for the insertion of metal heteroatoms into a layered zeolite precursor RUB-36 by interlayer expansion. Through this methodology, Sn-JHP-1, Fe-JHP-1, Zn-JHP-1 and Co-JHP-1 zeolites are successfully synthesized. Various characterization techniques confirm the isolated metal species (Sn, Fe, Zn, and Co) within the zeolite framework. The insertion of metal heteroatoms leads to a novel zeolitic structure and broadens catalytic functionality of layered silicates. This generalized methodology for the insertion of metal heteroatoms into a layered zeolite precursor by interlayer expansion is described in this work and

thus the obtained zeolite samples have significant potential applications for industrial catalysis in the near future.

**Supplementary Materials:** The following are available online at http://www.mdpi.com/2073-4352/10/6/530/s1, Synthesis of Zn-JHP-1, calcined Zn-JHP-1 (Zn-JHP-2), Fe-JHP-1, calcined Fe-JHP-1 (Fe-JHP-2), Co-JHP-1 and calcined Co-JHP-1 (Co-JHP-2); Figure S1: XRD pattern of Sn-JHP-2-r.

**Author Contributions:** Conceptualization and writing, C.B. and L.Z.; methodology, J.Z., X.W. and Z.F.; investigation, J.Q., F.Z. and L.Y. All authors have read and agreed to the published version of the manuscript.

**Funding:** This research was funded by the National Natural Science Foundation of China (21902065, and 21802053), the Hundred Youth Project of Jiaxing University (CD70619032) and Jinhua Science and Technology Bureau (2019-4-165, 2018-3-002, 2017-4-001, and 2019-4-168).

**Conflicts of Interest:** The authors declare no conflict of interest.

## References

1. Dusselier, M.; Davis, M.E. Small-Pore Zeolites: Synthesis and Catalysis. *Chem. Rev.* **2018**, *118*, 5265–5329. [CrossRef] [PubMed]
2. Martinez, C.; Corma, A. Inorganic molecular sieves: Preparation, Modification and Industrial Application in Catalytic Processes. *Coord. Chem. Rev.* **2011**, *255*, 1558–1580. [CrossRef]
3. Wu, Q.; Meng, X.; Gao, X.; Xiao, F.-S. Solvent-free Synthesis of Zeolites: Mechanism and Utility. *Acc. Chem. Res.* **2018**, *51*, 1396–1403. [CrossRef] [PubMed]
4. Wang, N.; Sun, Q.; Bai, R.; Li, X.; Guo, G.; Yu, J. In Situ Confinement of Ultrasmall Pd Clusters within Nanosized Silicalite-1 Zeolite for Highly Efficient Catalysis of Hydrogen Generation. *J. Am. Chem. Soc.* **2016**, *138*, 7484–7487. [CrossRef]
5. Brandenberger, S.; Krocher, O.; Tissler, A.; Althoff, R. The State of the Art in Selective Catalytic Reduction of $NO_x$ by Ammonia using Metal-Exchanged Zeolite Catalysts. *Catal. Rev.* **2008**, *50*, 492–531. [CrossRef]
6. Ouyang, X.; Hwang, S.; Xie, D.; Rea, T.; Zones, S.I.; Katz, A. Heteroatom-Substituted Delaminated Zeolites as Solid Lewis Acid Catalysts. *ACS Catal.* **2015**, *5*, 3108–3119. [CrossRef]
7. Jin, Z.; Wang, L.; Zuidema, E.; Mondal, K.; Zhang, M.; Zhang, J.; Wang, C.; Meng, X.; Yang, H.; Mesters, C.; et al. Hydrophobic Zeolite Modification for in Situ Peroxide Formation in Methane Oxidation to Methanol. *Science* **2020**, *367*, 193–197.
8. Jones, A.; Carr, R.; Zones, S.I.; Iglesia, E. Acid Strength and Solvation in Catalysis by MFI Zeolites and Effects of the Identity, Concentration and Location of Framework Heteroatoms. *J. Catal.* **2014**, *312*, 58–68. [CrossRef]
9. Shamzhy, M.; Opanasenko, M.; Concepcion, P.; Martínez, A. New Trends in Tailoring Active Sites in Zeolite-Based Catalysts. *Chem. Soc. Rev.* **2019**, *48*, 1095–1149. [CrossRef]
10. Ryu, T.; Hong, S. Iron-exchanged UZM-35: An Active $NH_3$-SCR Catalyst at Low Temperatures. *Appl. Catal. B Environ.* **2020**, *266*, 118622. [CrossRef]
11. Zhu, Z.; Xu, H.; Jiang, J.; Guan, Y.; Wu, P. Sn-Beta Zeolite Hydrothermally Synthesized via Interzeolite Transformation as Efficient Lewis Acid Catalyst. *J. Catal.* **2017**, *352*, 1–12. [CrossRef]
12. Wang, C.; Zhang, J.; Qin, G.; Wang, L.; Zuidema, E.; Yang, Q.; Dang, S.; Yang, C.; Xiao, J.; Meng, X.; et al. Direct Conversion of Syngas to Ethanol within Zeolite Crystals. *Chem* **2020**, *6*, 1–12. [CrossRef]
13. Marler, B.; Gies, H. Hydrous layer silicates as precursors for zeolites obtained through topotactic condensation: A review. *Eur. J. Mineral.* **2012**, *24*, 405–428. [CrossRef]
14. Camblor, M.A.; Corell, C.; Corma, A.; Diaz-Cabanas, M.-J.; Nicolopoulos, S.; Gonzalez-Calbet, J.M.; Vallet-Regi, M. A New Microporous Polymorph of Silica Isomorphous to Zeolite MCM-22. *Chem. Mater.* **1996**, *8*, 2415–2417. [CrossRef]
15. Roth, W.; Nachtigall, P.; Morris, R.; Cejka, J. Two-Dimensional Zeolites: Current Status and Perspectives. *Chem. Rev.* **2014**, *114*, 4807–4837. [CrossRef] [PubMed]
16. Inagaki, S.; Yokoi, T.; Kubota, Y.; Tatsumi, T. Unique Adsorption Properties of Organic-Inorganic Hybrid Zeolite IEZ-1 with Dimethylsilylene Moieties. *Chem. Commun.* **2007**, 5188–5190. [CrossRef]
17. Wu, P.; Ruan, J.; Wang, L.; Wu, L.; Wang, Y.; Liu, Y.; Fan, W.; He, M.; Terasaki, O.; Tatsumi, T. Methodology for Synthesizing Crystalline Metallosilicates with Expanded Pore Windows through Molecular Alkoxysilylation of Zeolitic Lamellar Precursors. *J. Am. Chem. Soc.* **2008**, *130*, 8178–8187. [CrossRef]

18. Zhao, Z.; Zhang, W.; Ren, P.; Han, X.; Muller, U.; Yilmaz, B.; Feyen, M.; Gies, H.; Xiao, F.-S.; De Vos, D.; et al. Insights into the Topotatic Conversion Process from Layered Silicate RUB-36 to FER-type Zeolite by Layer Reassembly. *Chem. Mater.* **2013**, *25*, 840–847. [CrossRef]
19. Gies, H.; Muller, U.; Yilmaz, B.; Tatsumi, T.; Xie, B.; Xiao, F.-S.; Bao, X.; Zhang, W.; De Vos, D. Interlayer Expansion of the Layered Zeolite Precursor RUB-39: A Universal Method To Synthesize Functionalized Microporous Silicates. *Chem. Mater.* **2011**, *23*, 2545–2554. [CrossRef]
20. Wu, P.; Nuntasri, D.; Ruan, J.; Liu, Y.; He, M.; Fan, W.; Terasaki, O.; Tatsumi, T. Delamination of Ti-MWW and High Efficiency in Epoxidation of Alkenes with Various Molecular Sizes. *J. Phys. Chem. B* **2004**, *108*, 19126–19131. [CrossRef]
21. Gies, H.; Muller, U.; Yilmaz, B.; Feyen, M.; Tatsumi, T.; Imai, H.; Zhang, H.; Xie, B.; Xiao, F.-S.; Bao, X.; et al. Interlayer Expansion of the Hydrous Layer Silicate RUB-36 to a Functionalized, Microporous Framework Silicate: Crystal Structure Analysis and Physical and Chemical Characterization. *Chem. Mater.* **2012**, *24*, 1536–1545. [CrossRef]
22. De Baerdemaeker, T.; Feyen, M.; Vanbergen, T.; Muller, U.; Yilmaz, B.; Xiao, F.-S.; Zhang, W.; Yokoi, T.; Bao, X.; De Vos, D.; et al. From Layered Zeolite Precursors to Zeolites with a Three-Dimensional Porosity: Textural and Structural Modifications through Alkaline Treatment. *Chem. Mater.* **2015**, *27*, 316–326. [CrossRef]
23. Xiao, F.-S.; Xie, B.; Zhang, H.; Wang, L.; Meng, X.; Zhang, W.; Bao, X.; Yilmaz, B.; Muller, U.; Gies, H.; et al. Interlayer-Expanded Microporous Titanosilicate Catalysts with Functionalized Hydroxyl Groups. *ChemCatChem* **2011**, *3*, 1442–1446. [CrossRef]
24. De Baerdemaeker, T.; Gies, H.; Yilmaz, B.; Muller, U.; Feyen, M.; Xiao, F.-S.; Zhang, W.; Yokoi, T.; Bao, X.; De Vos, D. A New Class of Solid Lewis Acid Catalysts Based on Interlayer Expansion of Layered Silicates of the RUB-36 type with Heteroatoms. *J. Mater. Chem. A* **2014**, *2*, 9709–9717. [CrossRef]
25. Gies, H.; Feyen, M.; De Baerdemaker, T.; De Vos, D.; Yilmaz, B.; Muller, U.; Meng, X.; Xiao, F.S.; Zhang, W.; Yokoi, T.; et al. Interlayer Expansion Using Metal-Linker Units: Crystalline Microporous Silicate Zeolites with Metal Centers on Specific Framework Sites. *Microporous Mesoporous Mater.* **2016**, *222*, 235–240. [CrossRef]
26. Bian, C.; Wu, Q.; Zhang, J.; Pan, S.; Wang, L.; Meng, X.; Xiao, F.-S. Interlayer Expansion of the Layered Zeolite Precursor COK-5 with $Sn(acac)_2Cl_2$. *J. Eng. Chem.* **2015**, *24*, 642–645.
27. Wang, L.; Zhang, J.; Wang, X.; Zhang, B.; Ji, W.; Meng, X.; Li, J.; Su, D.; Bao, X.; Xiao, F.-S. Sulfonated hollow sphere carbon as an efficient catalyst for acetalisation of glycerol. *J. Mater. Chem. A* **2014**, *2*, 3725–3729. [CrossRef]
28. Luo, H.; Bui, L.; Gunther, W.; Min, E.; Roman-Leshkov, Y. Synthesis and Catalytic Activity of Sn-MFI Nanosheets for the Baeyer-Villiger Oxidation of Cyclic Ketones. *ACS Catal.* **2012**, *2*, 2695–2699. [CrossRef]
29. Tang, B.; Dai, W.; Wu, G.; Guan, N.; Li, L.; Hunger, M. Improved Post-Synthesis Strategy to Sn-Beta Zeolites as Lewis Acid Catalysts for the Ring-Opening Hydration of Epoxides. *ACS Catal.* **2014**, *4*, 2801–2810. [CrossRef]
30. Yong, G.; Zhang, Y.; Ying, J. Efficient Catalytic System for the Selective Production of 5-Hydroxymethylfurfural from Glucose and Fructose. *Angew. Chem. Int. Ed.* **2008**, *47*, 9345–9348. [CrossRef]
31. Pagan-Torres, Y.; Wang, T.; Gallo, J.; Shanks, B.; Dumesic, J. Production of 5-Hydroxymethylfurfural from Glucose Using a Combination of Lewis and Brønsted Acid Catalysts in Water in a Biphasic Reactor with an Alkylphenol Solvent. *ACS Catal.* **2012**, *2*, 930–934. [CrossRef]
32. Stahlberg, T.; Grau Sorensen, M.; Riisager, A. Direct conversion of glucose to 5-(hydroxymethyl) furfural in ionic liquids with lanthanide catalysts. *Green Chem.* **2010**, *12*, 321–325. [CrossRef]
33. Rami, N.; Amin, N. Catalytic Conversion of Carbohydrate Biomass in Ionic Liquid to 5-(Hydroxymethyl) Furfural and Levulinic Acid: A Review. *BioEnergy Res.* **2020**. [CrossRef]
34. Stahlberg, T.; Rodriguez-Rodriguez, S.; Fristrup, P.; Riisager, A. Metal-free Dehydration of Glucose to 5-(Hydroxymethyl) Furfural in Ionic Liquids with Boric Acid as a Promoter. *Chem. Eur. J.* **2011**, *17*, 1369. [CrossRef]
35. Hou, Q.; Zhen, M.; Li, W.; Liu, L.; Liu, J.; Zhang, S.; Nie, Y.; Bai, X.; Ju, M. Efficient Catalytic Conversion of Glucose into 5-Hydroxymethylfurfural by Aluminum Oxide in Ionic Liquid. *Appl. Catal. B Environ.* **2019**, *253*, 1–10. [CrossRef]
36. Hou, Q.; Zhen, M.L.; Chen, Y.; Huang, F.; Zhang, S.; Li, W.; Ju, M. Tin Phosphate as a Heterogeneous Catalyst for Efficient Dehydration of Glucose into 5-Hydroxymethylfurfural in Ionic Liquid. *Appl. Catal. B Environ.* **2018**, *224*, 183–193. [CrossRef]

37. Wang, L.; Sang, S.; Meng, S.; Zhang, Y.; Qi, Y.; Liu, Z. Direct Synthesis of Zn-ZSM-5 with Novel Morphology. *Mater. Lett.* **2007**, *61*, 1675–1678. [CrossRef]
38. Ni, Y.; Sun, A.; Wu, X.; Hai, G.; Hu, J.; Li, T.; Li, G. The Preparation of Nano-Sized H [Zn, Al] ZSM-5 Zeolite and Its Application in the Aromatization of Methanol. *Microporous Mesoporous Mater.* **2011**, *143*, 435–442. [CrossRef]
39. Xavier, K.; Chacko, J.; Mohammed Yusuff, K. Zeolite-Encapsulated Co(II), Ni(II) and Cu(II) Complexes as Catalysts for Partial Oxidation of Benzyl Alcohol and Ethylbezene. *Appl. Catal. A Gen.* **2004**, *258*, 251–259. [CrossRef]
40. Janas, J.; Shishido, T.; Che, M.; Dzwigaj, S. Role of Tetrahedral Co(II) sites of CoSiBEA Zeolite in the Selective Catalytic Reduction of NO: XRD, UV-Vis, XAS and Catalysis Study. *Appl. Catal. B Environ.* **2009**, *89*, 196–203. [CrossRef]